

Response to reviewer#1

Thanks for the reviewer's helpful and insightful suggestions! The comments are addressed point-by-point and responses are listed below.

**Comments:** New particle formation contributes to more than half of CCN and thereby is important for climate. This work conducts the vertical measurements of particle number size distribution on a moving cabin of a 350 m tower. This kind of experiment is interesting and can improve the understanding of the vertical distributions of new particle formation (NPF) in the urban environment. However, I believe that the evidence on the occurrence of nucleation at 240 m or upper boundary layer in this manuscript is not enough. A major revision is needed before considering publication in ACP.

**Reply:** Thanks for the comments.

**Comments:** Line 44-50: It is not suitable to put equations of sulfuric acid proxy and CS and the explanation of these two equations in the Introduction. I suggest moving those to Section 2.

**Reply:** Thanks for the comments and helpful suggestions. The corresponding equations were moved to section 2.5. We added a section to describe how the sulfate acid concentration can be influenced by the photolysis ratio in section 2.5.

**Comments:** Line 79-89: The time resolutions of instruments need to be presented. How do they compare with the lifting speed of the cabin?

**Reply:** Thanks for the comment. The time resolutions were added in the corresponding text. The cabin moved around 10 meters every minute in altitude. Aerosol PNSD was measured using a scanning mobility particle size every five minutes. Aerosol scattering coefficient ( $\sigma_{sca}$ ) were measured by an Aurora 3000 nephelometer with a time resolution of one minute. The nitrogen dioxide (NO<sub>2</sub>) was measured every minute based on its absorbance at 405 nm with a low-power lightweight instrument (model 405 nm, 2B Technology, USA). The nitrogen monoxide (NO) was measured by adding an excess of ozone with another power lightweight instrument (model 106-L, 2B Technology, USA) with a time resolution of one minute. All of the data were averaged with a time resolution of five minutes.

**Comments:** Line119-121: I suggest the author gives the description of the changes of the TUV model in SI.

**Reply:** Thanks for the comment. We added a brief description of the changes of the TUV model in the manuscript.

In the TUV model, the input of the aerosol optical properties are the aerosol optical depths at the wavelength of 550 nm and the column-averaged SSA. The profiles of the  $\sigma_{sca}$  are calculated assuming that the aerosol  $\sigma_{sca}$  are proportional to those measured by Elterman et al. (1968). The g values are set to be fixed as 0.61. Some changes were made in the source code of the TUV model. In our model, the author-defined aerosol  $\sigma_{sca}$  profiles, SSA profiles and g profiles can be used as the input of the model. Therefore, the J(NO<sub>2</sub>) and J(O<sup>1</sup>D) profiles with different aerosol optical profiles (including aerosol  $\sigma_{sca}$ , SSA, and g) can be estimated.

**Comments:** Line 144-145: What are the differences in PNSD when cabin moving upward and downward? Because the time is close when cabin moving upward and downward, I would suppose the PNSDs are similar. If so, I suggest the author merges the upward and downward PNSD. If not, please explain the reasons.

**Reply:** Thanks for the comment. The PNSD when the cabin moving upward and downward is the time corresponds to different measurement time and the time interval differs for different height. The time shown in Fig. 2 (Fig. S3) corresponds to the time when the cabin begins to move up (down) from the ground (240 m height). The time intervals are approximately one hour and half an hour for the measured aerosol PNSD at the ground and the height of about 120 m respectively when the cabin moves upward and downward in one cycle. The aerosol PNSD may vary significantly within an hour. Therefore, it is not appropriate to merge the upward and downward PNSD. The main conclusions in the development of aerosol PNSD with time are almost the same when the cabin moves upward and downward, and thus we placed the measured PNSD when cabin moving upward downward in different figure.

**Comments:** Section 3.2: In this section, the authors discussed the stronger nucleation in the upper boundary layer. However, some more evidences are needed for this conclusion.

1. The maximum altitude of this vertical measurement is 240 m. The boundary layer height is around 1500 m in winter. Therefore, I don't think this measurement can represent the

situations of upper boundary layer even in winter. I suggest the author uses ‘above the urban canopy’ instead of the ‘upper boundary layer’.

**Reply:** Thanks for the comment. We agree with the reviewer that it is not appropriate to use the ‘upper boundary layer’. We replaced the “upper boundary layer” as the “upper mixing layer” in the manuscript for two reasons. The first is that the statistical results of the mixed layer height in Beijing winter is  $493 \pm 131$  m (Zhu et al., 2018). The corresponding height is even lower during the haze episodes (Wang et al., 2018). Our measurement covers about half of the mixed layer height. The second is that despite that the maximum altitude of our vertical measurement is 240 m, our general framework of the development of the atmospheric mixing layer is consistent with our measurements and previous studies (Zhu et al., 2018). As long as the aerosol was uniformly distributed in the mixed layer due to the strong turbulence, our main conclusion that the nucleation processing in the upper mixed layer is stronger than that at the ground is applicable.

**Comments:** 2. I suggest the author give the legend of each profile in Fig.3.

**Reply:** Thanks for the helpful suggestions. We added the legend of each profile in Fig. 3 and Fig. 4.

**Comments:** 3. Are there any ground-based measurements on this day? From the ground-based measurements, is it a new particle formation event day?

**Reply:** Thanks for the comment. During the field campaign, there was no ground-based measurement of the aerosol PNSD. From the measured PNSD at the ground in Fig. 2, we think it is not a new particle formation event day.

**Comments:** 4. The ratio of nucleation mode particles number concentrations to Aitken mode particles number concentrations increased at 16:15. Does the author mean the nucleation occur at late afternoon? Most of NPF events start at noontime when the solar radiation is strong. Although the ratio increased at 16:15, the PNSD shown in Fig. 2 is not a typical PNSD of nucleation.

**Reply:** Thanks for the comment. We don't mean that the nucleation occurs in the afternoon. We agree with the reviewer that most of the NPF events start at noontime or in the morning when the solar radiation is strong. In fig. 2, we want to show that the measured ratio of the nucleation mode particle number concentrations to Aitken mode aerosol number concentration increase with height in the afternoon. The nucleation process in the upper boundary layer is stronger than that at the ground. The difference in the aerosol number concentration ratio of nucleation mode to Aitken mode is not observed in the noontime because the turbulence in the noontime is so strong that the particles in the vertical distribution are well mixed. The turbulence is rather weak in the late afternoon and then we can observe more aerosol number concentrations in nucleation mode in the late afternoon.

The fig. 2 is not a typical PNSD of nucleation because the measured PNSD results from the long differential mobility analyzer (DMA) at the size range smaller than 15 nm, where the PNSD is always underestimated. Our measurement results are in accordance with the

previous measurement of PNSD (Du et al., 2018; Qi et al., 2019). In the related reference, the PNSD is not a typical PNSD.

**Comments:** 5. Although the wind speed is low during the measurement, the wind direction changed at around 16:00. Is it possible that the change of the air masses caused the observed phenomenon? Are there intensive local anthropogenic emissions to the southwest of measurement site?

**Reply:** Thanks for the comments. The wind direction changed at around 14:00. The measured aerosol PNSDs were almost the same at 13:20, 13:50, 14:25, and 15:05 as the turbulence in the noon was strong and the aerosols were uniformly distributed. Thus, the observed phenomenon is not likely to be caused by the change of the air mass. The local anthropogenic emissions may influence the PNSD at the ground in the morning as shown in Fig. 2(a), (b). However, it is not likely that the local anthropogenic emissions may influence the observed phenomenon in fig. 2(e), (f) and (g).

**Comments:** Line219-220: The author needs to give some evidences or cite some references here. SO<sub>2</sub> can be from the power plant and the NO<sub>x</sub> is most from the vehicle emissions. They may have different vertical distributions.

**Reply:** Thanks for the helpful suggestions. We added some discussion in the corresponding manuscript. Both the NO<sub>x</sub> and SO<sub>2</sub> were mainly from the ground emission. The SO<sub>2</sub> tends to have a longer lifetime than that of NO<sub>x</sub> (Steinfeld, 1998). Thus, the SO<sub>2</sub> tends to be more uniform distributed within the boundary layer than NO<sub>x</sub> when the turbulence is strong. We

found that the NO<sub>x</sub> is uniformly distributed at noon and in the afternoon. Therefore, it is reasonable that we assume the SO<sub>2</sub> is uniformly distributed at noon and in the afternoon.

**Comments:** Figure 4: The concentration of NO<sub>x</sub> can be more than 200 ppbv. Is it a heavy pollution day?

**Reply:** Thanks for the comment. The NO<sub>x</sub> is high because the measurement location is close to the vehicle source. We replot Fig. 4 and found that the high NO<sub>x</sub> concentration happens after 18:00 and these profiles are removed from Fig. 4. During the measurement, the NO<sub>x</sub> concentration is about 120 ppbv. It is not a heavy pollution day on January 19, 2019, and the measured mean PM<sub>2.5</sub> in Beijing on this day is only 47 µg/m<sup>3</sup>.

**Comments:** Line 243-248: The vertical measurement in this study is from ground level to 240 m. However, in this section the author takes lots of words on the differences between the situations of ground level and the top of boundary layer. From Fig. 5, the [OH] didn't increase that much at 240 m compared to ground level.

**Reply:** Thanks for the comments. In this section, we assumed that the aerosols within the mixing layer were well mixed and uniformly distributed. The main purpose of our work is to propose a framework that the nucleation processing in the upper mixing layer is stronger than that at the ground. Despite that our measurement height is from ground level to 240 m, the main conclusion of the development of the mixing layer during the daytime applies to the whole mixing layer. It is reasonable we compare the differences between the situations of ground level and the top of the boundary layer.

The [OH] increased from  $6.39 \times 10^6 \text{ cm}^3$  at the ground to  $11.23 \times 10^6 \text{ cm}^3$  at the top of the mixing layer by 76.7% and increased from  $6.39 \times 10^6 \text{ cm}^3$  at the ground to  $9.3 \times 10^6 \text{ cm}^3$  at 240 m height by 44.8% when the mixing layer type is B with a mixing layer height of 500 m. Thus the [OH] increased significantly with height.

**Comments:** Line 247-254: I don't think a schematic graph is needed here. Moreover, the schematic graph is not well presenting the author's view. The loop showing in Fig. 6 is a positive feedback loop, but I think it is not the case in this study.

**Reply:** Thanks for the comments. We agree with the reviewer that Fig. 6 is not needed and we removed Fig. 6 in the manuscript.

**Comments:** Section 3.4: In this section, the author discussed the vertical profiles of photolysis rates for 4 types of aerosol profiles. But most of discussions are about the comparisons between the top of boundary layer and ground, which is not related to the measurement of this study. The author also needs to consider the vertical distribution of  $\text{SO}_2$ , CS, VOCs when discussing the reasons of the NPF occurring at high altitude.

**Reply:** Thanks for the comments. In this section, we assumed that the aerosols within the mixing layer were well mixed and uniformly distributed. The main purpose of our work is to propose a framework that the nucleation processing in the upper mixing layer is stronger than that at the ground. Despite that our measurement is from ground level to 240 m, the main conclusion of the development of the mixing layer during the daytime applies to the whole mixing layer. It is reasonable we compare the differences between the situations of



ground level and the top of the boundary layer. In our framework, we focus on the influence of aerosol-radiation interaction on the nucleation processing within the mixing layer, the SO<sub>2</sub>s, CS, and VOCs are assumed to be uniformly distributed within the mixing layer.

Du, P., Gui, H., Zhang, J., Liu, J., Yu, T., Wang, J., Cheng, Y., and Shi, Z.: Number size distribution of atmospheric particles in a suburban Beijing in the summer and winter of 2015, *Atmospheric Environment*, 186, 32-44, 10.1016/j.atmosenv.2018.05.023, 2018.

Elterman, L., Wexler, R., and Chang, D.: COMPARISON OF AEROSOL MEASUREMENTS OVER NEW MEXICO WITH ATMOSPHERIC FEATURES, *Journal of the Optical Society of America*, 58, 741-&, 1968.

Qi, X., Ding, A., Nie, W., Chi, X., Huang, X., Xu, Z., Wang, T., Wang, Z., Wang, J., Sun, P., Zhang, Q., Huo, J., Wang, D., Bian, Q., Zhou, L., Zhang, Q., Ning, Z., Fei, D., Xiu, G., and Fu, Q.: Direct measurement of new particle formation based on tethered airship around the top of the planetary boundary layer in eastern China, *Atmospheric Environment*, 209, 92-101, 10.1016/j.atmosenv.2019.04.024, 2019.

Steinfeld, J. I.: *Atmospheric Chemistry and Physics: From Air Pollution to Climate Change*, *Environment: Science and Policy for Sustainable Development*, 40, 26-26, 10.1080/00139157.1999.10544295, 1998.

Wang, Q., Sun, Y., Xu, W., Du, W., Zhou, L., Tang, G., Chen, C., Cheng, X., Zhao, X., Ji, D., Han, T., Wang, Z., Li, J., and Wang, Z.: Vertically resolved characteristics of air pollution during two severe winter haze episodes in urban Beijing, China, *Atmospheric Chemistry and Physics*, 18, 2495-2509, 10.5194/acp-18-2495-2018, 2018.

Zhu, X., Tang, G., Guo, J., Hu, B., Song, T., Wang, L., Xin, J., Gao, W., Munkel, C., Schäfer,

K., Li, X., and Wang, Y.: Mixing layer height on the North China Plain and meteorological evidence of serious air pollution in southern Hebei, *Atmospheric Chemistry and Physics*, 18, 4897-4910, 10.5194/acp-18-4897-2018, 2018.

Response to reviewer#2

Thanks for the reviewer's helpful suggestions! The comments are addressed point-by-point and responses are listed below.

**Comments:** The research on new particle formation (NPF) is of great importance considering its vital role in modulating the cloud condensation nuclei. While NPF has been widely studied, the authors primarily focus on the development of aerosol size distribution among different altitudes as well as the impact of aerosol-radiation on NPF. The analysis angle is unique and the manuscript is well written. I have a few comments prior to the acceptance of the manuscript for publication.

**Reply:** Thanks for the comments.

**Comments:** Major comments: 1. A typical NPF figure ( $dN/d\log D_p$  vs. time) at a few selected altitudes might be helpful for readers to understand the evolution of NPF along with time and altitude.

2. In the abstract, the authors hypothesized that the nucleation processing in the upper boundary layer should be stronger than that at the ground. Since the observational PNSD in the vertical direction is available, I am wondering whether the authors can calculate the formation rate directly. In this way, one can easily identify whether the nucleation processing over the upper altitude is higher than that at the ground.

**Reply:** Thanks for the comment. The reviewer gave insightful suggestions for better understanding the evolution of NPF. As shown in Fig. 2 and Fig. S3, we measured only 16 PNSD profiles on January 19, 2019. The time interval is so large that the typical NPF figure

at different altitudes is not available. Calculating the formation rate is not appropriate as the measured aerosol PNSD changed significantly (Cai and Jiang, 2017) with the development of the mixing layer.

Minor comments:

**Comments:** Line 120: Some changes were made in the source code of the TUV model so that the model can calculate the J(NO<sub>2</sub>) and J(O<sup>1</sup>D) profiles. A bit more information is useful. For instance, a few more words on what major changes have been made.

**Reply:** Thanks for the comment. We added a brief description of the changes of the TUV model in the manuscript.

In the TUV model, the input of the aerosol optical properties are the aerosol optical depths at the wavelength of 550 nm and the column-averaged SSA. The profiles of the  $\sigma_{sca}$  are calculated assuming that the aerosol  $\sigma_{sca}$  are proportional to those measured by Elterman et al. (1968). The g values are set to be fixed as 0.61. Some changes were made in the source code of the TUV model. In our model, the author-defined aerosol  $\sigma_{sca}$  profiles, SSA profiles and g profiles can be used as the input of the model. Therefore, the J(NO<sub>2</sub>) and J(O<sup>1</sup>D) profiles with different aerosol optical profiles (including aerosol  $\sigma_{sca}$ , SSA, and g) can be estimated.

**Comments:** Line 123: Altitude, Please revise to altitudes

**Reply:** Thanks for the comment. We revised the word.

**Comments:** Line 132 (Line 193; 205;304): Transportation Please revise to transport.

**Reply:** Thanks for the comment. We revised the corresponding words.

**Comments:** Line 144 for different altitudes and a different time. Please revise to for different altitudes and time

**Reply:** Thanks for the comment. We revised this sentence.

**Comments:** Line 159 These particles were still not well mixed at the range between 0 and 240 m until 11:20. From Fig. 2, it does not seem to show the mixing at 11:20. Is it something not shown in the figure?

**Reply:** Thanks for the comment. The time should be 10:20. We revised the text in the corresponding manuscript.

**Comments:** Line 183 (Line 479;295) different times, Please revise to: different time

**Reply:** Thanks for the comment. We revised the corresponding words.

**Comments:**Line 185: The ratio on the ground surface decreased. It is not clear that the ground decreased compared to ??

**Reply:** Thanks for the comment. We want to say that the ratio at the ground decreased over time during 8:00 and 10:00 in the morning.

**Comments:** Line 196 later Should be late; if the authors only want to emphasize afternoon, the word "later" should be removed.

**Reply:** Thanks for the comment. We revised the words into “late afternoon”.

**Comments:** Line 266-270 The authors list the altitude of boundary layer height of either 1000 or 500 meters. Please clarify whether these heights are the exact boundary layer heights or approximate altitude? Or they represent a range, i.e., less than 1000 meters?

**Reply:** Thanks for the comment. The boundary layer heights of 1000 or 500 meters are the exact boundary layer heights. We made some revisions in the corresponding lines.

Cai, R., and Jiang, J.: A new balance formula to estimate new particle formation rate: reevaluating the effect of coagulation scavenging, *Atmospheric Chemistry and Physics*, 17, 12659-12675, 10.5194/acp-17-12659-2017, 2017.

Elterman, L., Wexler, R., and Chang, D.: COMPARISON OF AEROSOL MEASUREMENTS OVER NEW MEXICO WITH ATMOSPHERIC FEATURES, Journal of the Optical Society of America, 58, 741-&, 1968.

# Impact of aerosol-radiation interaction on new particle formation

Gang Zhao<sup>1</sup>, Yishu Zhu<sup>1</sup>, Zhijun Wu<sup>1</sup>, Taomou Zong<sup>1</sup>, Jingchuan Chen<sup>1</sup>, Tianyi Tan<sup>1</sup>, Haichao Wang<sup>1</sup>, Xin Fang<sup>1</sup>, Keding Lu<sup>1</sup>, Chunsheng Zhao<sup>2</sup>, Min Hu<sup>1\*</sup>

1 State Key Joint Laboratory of Environmental Simulation and Pollution Control, International Joint Laboratory for Regional Pollution Control, Ministry of Education (IJRC), College of Environmental Sciences and Engineering, Peking University, Beijing, 100871, China

2 Department of Atmospheric and Oceanic Sciences, School of Physics, Peking University, Beijing, 100871, China

\*Correspondence author: Min Hu (minhu@pku.edu.cn)

## Abstract

New particle formation (NPF) is thought to contribute to half of the global cloud condensation nuclei. A better understanding of the NPF at different altitudes can help assess the impact of NPF on cloud formation and corresponding physical properties. However, NPF is not sufficiently understood in the upper ~~boundary layer~~mixing layer because previous studies mainly focus on ground-level measurements. In this study, the developments of aerosol size distribution at different altitudes are characterized based on the field measurement conducted in January 2019, in Beijing, China. We find that the partition of nucleation mode particles at the upper ~~boundary layer~~mixing layer is larger than that at the ground, which implies that the nucleation processing is more likely to happen in the upper



boundary layer mixing layer than that at the ground. Results of the radiative transfer model show that  
20 the photolysis rates of the nitrogen dioxide and ozone increase with altitude within the boundary-  
layer mixing layer, which leads to a higher concentration of sulfuric acid at the upper boundary-  
layer mixing layer than that at the ground. Therefore, the nucleation processing in the upper boundary-  
layer mixing layer should be stronger than that at the ground, which is consistent with our  
measurement results. Our study emphasizes the influence of aerosol-radiation interaction on the NPF.  
25 These results have the potential to improve our understanding of the source of cloud condensation  
nuclei in-on global scale due to the impacts of aerosol-radiation interaction.

## 1 Introduction

Atmospheric particles influence the earth's energy balance by directly interacting with the solar  
radiation and indirectly being activated as cloud condensation nucleation (CCN) (Ghan and Schwartz,  
30 2007). New particle formation (NPF) in the atmosphere and the herein coagulation may enable  
particles to grow larger than 60 nm, at which point aerosols can exert radiative effects on the solar  
radiation and act as CCN (Williamson et al., 2019; Shang et al., 2020). Some researchers find that the  
NPF is responsible for around half of the global CCN (Merikanto et al., 2009; Du et al.,  
2017; Kulmala et al., 2014). However, there is still considerable uncertainty about the magnitude that  
35 the NPF attribute to CCN (Kulmala et al., 2004; Merikanto et al., 2009; Zhang et al., 2012). A better  
understanding of the NPF at different altitudes can help assess the impact of NPF on cloud formation  
and corresponding radiative effects. However, the underlying mechanism of NPF at different  
altitudes was not well studied yet.

Nucleation requires sufficient amounts of precursor gases (Kulmala et al., 2004). Sulfuric acid  
 40 (H<sub>2</sub>SO<sub>4</sub>) is thought to be the most important precursor for NPF events (Weber et al., 1997,  
 1996; Weber et al., 2001; Stolzenburg et al., 2005; Kulmala and Markku, 2013). Knowledge in the  
 profile of H<sub>2</sub>SO<sub>4</sub> number concentrations ([H<sub>2</sub>SO<sub>4</sub>]) can help understand the NPF mechanism, while  
 the profile of the sulfuric acid is not well known due to the limitation of measurements.

~~The content of H<sub>2</sub>SO<sub>4</sub> in a pseudo-steady state can be calculated (Kulmala et al., 2001) with:~~

$$[H_2SO_4] = k[OH][SO_2]/CS \quad (1)$$

~~Where [OH] and [SO<sub>2</sub>] are the number concentrations of hydroxyl radical and sulfur dioxide,  
 respectively; CS is the condensation sink, which quantifies the limitation of NPF from existing  
 particles. It is calculated as (Maso et al., 2005):~~

$$CS = 2\pi D \sum \beta_m(D_{p,i}) D_{p,i} N_i \quad (2)$$

~~where N<sub>i</sub> is the particle concentration in the size D<sub>p,i</sub>. The D is the diffusion coefficient of the  
 H<sub>2</sub>SO<sub>4</sub> and the β<sub>m</sub> is the transition regime correction factor. The content of H<sub>2</sub>SO<sub>4</sub> in a  
 pseudo-steady state can be estimated by the number concentration of hydroxyl radical [OH], sulfur  
 dioxide [SO<sub>2</sub>] and aerosol condensation sink (CS) (Kulmala et al., 2001; Shang et al., 2020). The~~

[OH] is related to solar ultraviolet radiation (Rohrer and Berresheim, 2006). Previous studies found  
 55 that the profile of photolysis radiation varies significantly for different aerosol vertical distributions  
 and the ultraviolet radiation is highly related to the aerosol optical properties (Tao et al., 2014).  
 Therefore, the ambient aerosol-radiation interaction may exert a significant influence on the NPF

~~through by~~ determining the [OH] vertical profile. However, the influence of ultraviolet radiation on the NPF is not well understood.

60 In the past few decades, extensive measurements have been conducted at ground level to characterize the ambient aerosol particle number size distribution (PNSD) and then NPF events (Bullard et al.; Du et al., 2018; Peng et al., 2017; Malinina et al., 2017). Some studies suggest that the nucleation of fine particles can be altitude-dependent (Shang et al., 2018). High concentrations of nucleation-mode particles were found in the upper parts of the ~~boundary-layer~~mixing layer (Schobesberger et al., 2013). It is observed that the particle growth rate in the upper ~~boundary-~~mixing layer is larger than that on the ground (Du et al., 2017). Measurements from the tethered  
65 balloon also show that a large partition of 11-16 nm particles was generated from the top region of the ~~boundary-layer~~mixing layer, and was then rapidly mixed down throughout the ~~boundary-~~mixing layer (Chen et al., 2018; Platis et al., 2016). Aircrafts measurements (Wang et al.,  
70 2016; Zhao et al., 2020) also found that the free troposphere favors the NPF. Most of these studies, to our best knowledge, focus on the concentration of precursor gases, but not on the aerosol-radiation interaction.

In this study, we first demonstrate that the NPF is more likely to happen in the upper ~~boundary-~~mixing layer than in the near-ground surface layer based on field measurement of the aerosol  
75 PNSD profiles. We find that the tendency of NPF is well related to ultraviolet radiation, implying that the aerosol-radiation interaction is an important factor that influences the NPF.

## 2 Data and Methods

### 2.1 Field Measurement

The field measurements were carried from 17 to 19 January 2019 at the Institute of Atmospheric Physics (IAP), Chinese Academy of Sciences (39°18' N, 116°22' E), an urban site in Beijing China. Details of the measurement site can refer to Wang et al. (2018a), Chen et al. (2015), and Wang et al. (2018b). Vertical measurements were conducted from the tower-based platform, with a maximum of 350 m, on the IAP campus. All of the instruments were installed on a moving cabin of the tower, which moves up and down in altitudes between 0 and 240 m. The cabin moved around 10 meters every minute in altitude. Aerosol PNSD in the size range between 10 nm and 700 nm ~~were~~was measured using a scanning mobility particle size (SMPS; TSI Inc. 3010) every five minutes. Aerosol scattering coefficient ( $\sigma_{sca}$ ) at the wavelength of 450 nm, 525 nm, and 635 nm were measured by an Aurora 3000 nephelometer (Müller et al., 2011) with a time resolution of one minute. The nitrogen dioxide (NO<sub>2</sub>) was measured every minute based on its absorbance at 405 nm with a low-power lightweight instrument (model 405 nm, 2B Technology, USA). The nitrogen monoxide (NO) was measured by adding an excess of ozone with another power lightweight instrument (model 106-L, 2B Technology, USA) with a time resolution of one minute. The wind speed, wind direction, ambient relative humidity, and temperature were measured by a small auto meteorology station. This instrument can record the atmosphere pressure, which was used to retrieve the altitude information. All of the data were averaged with a time resolution of five minutes.

## 2.2 Lognormal fit of PNSD

For each of the measured PNSD, it is fitted by three lognormal distribution modes by:

$$N(Dp) = \sum_{i=1,2,3} \frac{N_i}{\sqrt{2\pi} \log(\sigma_{g,i})} \exp \left[ -\frac{\log(Dp) - \log(Dp_i)}{2 \log^2(\sigma_{g,i})} \right] \quad (31)$$

Where  $N_i$ ,  $\sigma_{g,i}$ , and  $Dp_i$  are the number concentration, geometric standard deviation, and geometric mean diameter of mode  $i$  respectively. Two examples of fitting the measured PNSD are shown in Fig. S1. The three modes with geometric diameter ranges of 10 ~ 25 nm, 25 ~ 100 nm, and 100 ~ 700 nm correspond to the nucleation mode, Aitken mode, and accumulation mode respectively. The nucleation particles mainly result from the nucleation process and the Aitken mode particles are from primary sources, such as traffic sources (Shang et al., 2018). The accumulation mode particles are correlated with secondary formation, which mainly represents the ambient pollution conditions (Wu et al., 2008).

## 2.3 Mie Model

Mie scattering model (Bohren and Huffman, 2007) is used to estimate the aerosol optical properties. When running the Mie model, aerosol PNSD, aerosol black carbon mass size distribution and refractive index are essential. The measured mean black carbon mass size distribution from Zhao et al. (2019) is adopted in this study, which is measured around 3 kilometers away from this site. The refractive index of the non-black carbon and black carbon aerosol component are  $1.64+0i$ , which is the measured mean aerosol refractive index measured at Beijing (paper in preparation), and  $1.96 + 0.66i$  (Zhao et al., 2017) respectively. The aerosol hygroscopic growth is not considered here because

115 the ambient relative humidity during the measurement was all the way lower than 30% as shown in  
fig. 1(b). With the measured different aerosol PNSD and above-mentioned information, we can  
calculate the corresponding aerosol optical properties, which contain the aerosol  $\sigma_{sca}$ , aerosol single  
scattering albedo (SSA) and asymmetry factor ( $g$ ).

## 2.4 TUV Model

120 The Tropospheric Ultraviolet-Visible radiation model (TUV), developed by Madronich and  
Flocke (1997), is an advanced transfer model with an eight-stream, discrete ordinate solver. This  
model can calculate the spectral irradiance, spectral actinic flux, and photo-dissociation frequencies  
in the wavelength range between 121 nm and 735 nm. In this study, the photolysis frequency of the  
nitrogen dioxide ( $J(\text{NO}_2)$ ) and ozone ( $J(\text{O}^1\text{D})$ ) were used for further study. Inputs of the TUV model  
125 are the aerosol optical depth and single scattering albedo (Tao et al., 2014). The cloud aerosol optical  
depth is set to be zero in this study. The output of the TUV model includes the profiles of  $J(\text{NO}_2)$  and  
 $J(\text{O}^1\text{D})$ .

130 In the TUV model, the inputs of the aerosol optical properties are the aerosol optical depths at the  
wavelength of 550 nm and the column-averaged SSA. The profiles of the  $\sigma_{sca}$  are calculated  
assuming that the aerosol  $\sigma_{sca}$  are proportional to those measured by Elterman et al. (1968). The  $g$   
values are set to be fixed as 0.61. Some changes were made in the source code of the TUV model. In  
our model, the author-defined aerosol  $\sigma_{sca}$  profiles, SSA profiles and  $g$  profiles can be used as the  
input of the model. Therefore, the  $J(\text{NO}_2)$  and  $J(\text{O}^1\text{D})$  profiles with different aerosol optical profiles

(including aerosol  $\sigma_{sca}$ , SSA, and g) can be estimated. ~~Some changes were made in the source code of the TUV model so that the model can calculate the  $J(NO_2)$  and  $J(O^1D)$  profiles with different aerosol optical profiles (including aerosol  $\sigma_{sca}$ , SSA, and g).~~

## 2.5 Influence of photolysis ratio on the $[H_2SO_4]$

The content of  $H_2SO_4$  in a pseudo-steady state can be calculated (Kulmala et al., 2001) with:

$$[H_2SO_4] = k[OH][SO_2]/CS \quad (2)$$

Where  $[OH]$  and  $[SO_2]$  are the number concentrations of hydroxyl radical and sulfur dioxide, respectively; CS is the condensation sink, which quantifies the limitation of NPF from existing particles. It is calculated as (Maso et al., 2005):

$$CS = 2\pi D \sum \beta_m(D_{p,i}) D_{p,i} N_i \quad (3)$$

where  $N_i$  is the particle concentration in the size  $D_{p,i}$ . The D is the diffusion coefficient of the  $H_2SO_4$  and the  $\beta_m$  is the transition regime correction factor. Based on the work of Ehhalt and Rohrer (2000), the  $[OH]$  can be calculated by:

$$[OH] = a[J(O^1D)]^\alpha [J(NO_2)]^\beta \frac{b[NO_2] + 1}{c[NO_2]^2 + d[NO_2] + 1} \quad (4)$$

With  $\alpha$ ,  $\beta$ , a, b, c, d equaling 0.83, 0.19,  $4.1 \times 10^9$ , 140, 0.41, and 1.7, respectively.

## 3 Results and Discussions

### 3.1 Aerosol PNSD at different altitudes and time

The measured aerosol PNSD profiles in the time range between 7:00 and 18:50 on January 18 were used for analysis, which contained eight different upward movement and downward movement of the cabin, respectively. Fig. 1 (a) gives detailed time-altitude information of each measurement. All of the time mentioned in the research corresponds to the local time zone.

On January 18, the measured ambient temperature and relative humidity ranges were  $-3^{\circ}\text{C} \sim 10^{\circ}\text{C}$  and  $13\% \sim 24\%$  respectively, which implied that the ambient air in the winter of Beijing ~~are~~is dry and cold. Aerosol hygroscopic growth was thus not considered in this study. The wind speeds during the measurement were lower than  $1\text{m/s}$ , and thus the measurement results of aerosol microphysical properties were hardly influenced by transportation.

During the measurement, the  $\sigma_{sca}$  varied between 0 and  $400\text{ Mm}^{-1}$ . It ranged between  $100\text{ Mm}^{-1}$  and  $200\text{ Mm}^{-1}$  on 18, January. We compared the measured  $\sigma_{sca}$  using the nephelometer and calculated  $\sigma_{sca}$  using the Mie scattering model and measured PNSD. The measured and calculated  $\sigma_{sca}$  show good consistency with slope values of 1.00, 0.95, and 0.89 for wavelengths of 450 nm, 525 nm, and 635 nm, respectively, as shown in Fig. S2. The calculated  $\sigma_{sca}$  values are slightly smaller than that of the measured ones because the measured aerosol PNSD only covers the aerosol diameter between 10 nm and 700 nm, while the measured  $\sigma_{sca}$  represents the optical properties of the whole population. The square of the correlation coefficients are 0.97, 0.97, and 0.97 for the above-mentioned different wavelengths. Our results demonstrate that the measured ambient aerosol PNSDs are reliable for further analysis.



170 The measured aerosol PNSD varied significantly for different altitudes and ~~a different~~ time. PNSD profiles in Fig. 2 corresponded to these ~~time~~ periods when the cabin moved upward. The corresponding downward PNSD profiles are shown in Fig. S2. In the early morning, the PNSD on the ground surface is substantially different for different altitudes. Particle number concentration on the ground surface can reach  $1.5 \times 10^4 \text{ cm}^{-3}$ , and the number concentrations peaked at smaller than 100  
175 nm. It was only  $8 \times 10^3 \text{ cm}^{-3}$  with peaking aerosol diameter at around 200 nm at a higher altitude ~~of~~ around 200 m. The solar radiation in the morning was very weak, therefore, the turbulence mixing of the aerosol among different altitudes was very weak. The initial emission from the ground surface cannot be mixed up to higher locations, and thus the aerosol number concentrations at the surface ~~was-were~~ larger than that at a higher level as shown in Fig. 2(a).

180 With the increment of solar radiation and ambient temperature, the turbulence mixing of ambient particles ~~s~~ became stronger. The aerosol PNSD at the surface decreased with time because the near ground particles were mixed up to a higher location as shown in Fig. 2(b) and (c). However, the aerosol PNSD at higher altitude increased with time due to the upcoming mixed aerosol particles from lower altitude. Therefore, the difference between the aerosol PNSD at different altitudes  
185 became smaller with the development of the ~~boundary layer~~ mixing layer as shown in Fig. 2 (b), (c), and (d). These particles were still not well mixed at the range between 0 and 240 m until ~~10~~4:20.

In the afternoon, the ~~boundary layer~~ mixing layer was well mixed with the increment of solar radiation and ambient temperature. The aerosol PNSD and PVSD were almost uniformly distributed as shown in Fig. 2 (e) and (f). However, the turbulence was relatively weak after 15:00 as the

190 measured PNSD and PVSD on the ground surface were slightly larger than that of a higher place. After 16:00, the turbulence was weaker because a larger difference between the PNSD at the ground surface and the higher level existed. The ambient particles were hardly mixed after the sunset. The measured aerosol PNSD profiles showed almost the same properties as that in the morning, with more aerosol particles located on the ground surface from emissions.

195 Overall, the measured PNSD profiles were highly related to the intensity of turbulence. When the turbulence was weak, the PNSD at the surface was different from that of upper levels because the initially emitted particles cannot be mixed up to a higher location. The PNSD tended to be uniformly distributed when the turbulence within the boundary layer mixing layer was strong.

### 3.2 Nucleation process in the upper boundary layer mixing layer

200 We calculated aerosol total number concentration for each measured PNSD ( $N_{\text{tot}}$ ) and the profiles of  $N_{\text{tot}}$  are shown in Fig. 3 (a). All of the profiles in Fig. 3 corresponded to these cases when the cabin is moving up. The  $N_{\text{tot}}$  profiles varied significantly with the development of the boundary layer mixing layer. In the morning, the  $N_{\text{tot}}$  in the surface (larger than  $2 \times 10^4 \text{ cm}^{-3}$ ) was larger than that at a higher level (lower than  $1 \times 10^4 \text{ cm}^{-3}$ ) because the turbulence is so weak that the initially emitted  
205 particles on the surface cannot be transported to the upper level. In the afternoon around 14:00 and 16:00, the aerosol was well mixed in the boundary layer mixing layer and  $N_{\text{tot}}$  was almost uniform with around  $1.2 \times 10^4$  per cubic centimeter. Afterward, the turbulence was weaker than that in the

early afternoon and again the emitted aerosols cannot reach the higher level. The profile of  $N_{\text{tot}}$  in the morning was similar to that in the late afternoon and night.

210 The number ratio profiles of nucleation mode to Aitken mode ( $N_1/N_2$ ) for different times are shown in Fig. 3(b) and summarized in Table 1. In the morning of 7:00, the ratio decreased from around 0.6 to 0.04 when the cabin moved up from 0 to 240 m. The ratio on the ground surface decreased over time because the temperature and turbulence increased when it came to 8:00-10:00 in the morning. However, the turbulence was not strong enough to mix all of the particles to upper  
215 levels to 240 nm. The ratio still decreased with altitude. In the afternoon, the boundary-layer mixing layer developed well and the ratios between 13:20 and 14:25 were almost uniformly distributed at different altitudes. However, we found that the ratio increased with altitude from 0.21 to 0.34 when it came to 16:15, which implied that more nucleation mode particles were formed in the upper level in the boundary-layer mixing layer. The increment of the ratio was hardly influenced by transportation  
220 because the wind speed during the measurement was all the time lower than 1 m/s as shown in Fig. 1(b).

To better configure the variations of PNSD, we calculated the aerosol number concentrations with the diameter between 10 and 25 nm ( $N_{10-25\text{nm}}$ ). The  $N_{10-25\text{nm}}$  profiles in Fig. 3(c) show almost the same trends with the number ratio of  $N_1$  to  $N_2$ . In the morning and late afternoon, the  $N_{10-25\text{nm}}$   
225 decreased with the altitude. The  $N_{10-25\text{nm}}$  in the early afternoon were uniformly distributed due to the strong mixing in the boundary-layer mixing layer. When it came to 16:15, the  $N_{10-25\text{nm}}$  at different altitudes were-was larger than that in the early afternoon. Most importantly,  $N_{10-25\text{nm}}$  increases with

altitude. The aerosol total volume at 16:15 does not increase with altitude because the nucleation produced particles are so small that they contribute negligibly to the aerosol total volume.

230 Based on the discussion above, we found that the total aerosol number concentrations increased slightly with altitude at 16:15. The number ratio of  $N_1$  to  $N_2$  and the  $N_{10-25\text{nm}}$  increased with altitude. The total volumes of the aerosol particles were almost the same at different altitudes. The variation of PNSD was hardly influenced by transport~~ation~~. Therefore, we concluded that the nucleation process was more likely to happen in the upper level of the ~~boundary-layer~~mixing layer than the  
235 ground surface. This phenomenon was not observed in the early afternoon because the turbulence in the early afternoon is so strong that the aerosol particles are well mixed in the ~~boundary-layer~~mixing layer.  
layer.

Many previous studies have reported the NPF events in the upper ~~boundary-layer~~mixing layer. The study in Platis et al. (2016) reported that the NPF originated at elevated altitude, and then being  
240 mixed down to the ground in Germany. The higher nucleation mode particle number concentrations were observed at the top region of the ~~boundary-layer~~mixing layer and were then rapidly mixed throughout the ~~boundary-layer~~mixing layer in America (Chen et al., 2018). Qi et al. (2019) also found the NPF at the top of the ~~boundary-layer~~mixing layer based on tethered airship measurements in eastern China. The NPF events were also observed at different altitudes in the North China Plain  
245 (Zhu et al., 2019).

### 3.3 Influence of Aerosol-radiation Interaction on NPF

Based on equation 42, the nucleation rate mainly depends on  $[OH]$ ,  $[SO_2]$ , and CS. The  $[SO_2]$  is not available at this measurement. However, we measured the  $[NO_x]$ , which is the sum of NO and  $NO_2$ . ~~The profiles of the  $[SO_2]$  and  $[NO_x]$  should be the same because both of them are mainly~~  
250 ~~emitted from the ground and then mixed up by turbulence. Both the  $[NO_x]$  and  $[SO_2]$  were mainly~~  
~~from the ground emission. The  $[SO_2]$  tend to have a longer lifetime than that of  $[NO_x]$  (Steinfeld,~~  
~~1998). Thus, the  $[SO_2]$  tends to be more uniform distributed within the boundary layer~~  
~~when the turbulence is strong.~~ The  $[NO_x]$  in the afternoon is almost uniformly distributed as shown  
in Fig. 4(a). Thus, the  $[SO_2]$  should be uniformly distributed in the afternoon within the ~~boundary-~~  
255 ~~layer~~mixing layer. The CS profiles, in Fig. 4(b), were almost uniformly distributed in the afternoon.  
Therefore, the  $[OH]$  is the only main factor that may result in different characteristics of NPF at  
different altitudes. From equation 4, the vertical distribution of  $J(O^1D)$ , and  $J(NO_2)$  played a  
significant influence on  $[OH]$  and further influence the NPF. However, the  $J(O^1D)$ , and  $J(NO_2)$   
were not measured. The TUV model was employed to estimate the  $J(O^1D)$ , and  $J(NO_2)$  for  
260 different aerosol profiles.

The input of the TUV needs the aerosol optical properties in the altitude range between 0-20 km.  
The parameterization of aerosol number concentration profiles by Liu et al. (2009) with aircraft  
measurement in Beijing is used in this study. Liu et al. (2009) found that number concentration  
constant within the ~~boundary-layer~~mixing layer, linearly decreasing within the transition layer and  
265 exponential decreasing above the transition layer; when the particles within the boundary are well  
mixed. The normalized aerosol PNSD (PNSD divided by total aerosol number concentration) was

assumed to be the same at different altitudes. The BC to total aerosol mass concentration ratio was also assumed to be the same at different altitudes (Ferrero et al., 2011). The  $\sigma_{sca}$ , SSA, and g profiles can be calculated by Mie theory under these assumptions (Zhao et al., 2017; Zhao et al., 2018).

The lines with squares in Fig. 5(a) and (b) provide the calculated photolysis rates of  $J(O^1D)$ , and  $J(NO_2)$  with a boundary layer mixing layer altitude of 1000 m. Results show that both the  $J(O^1D)$ , and  $J(NO_2)$  increase with altitude within the boundary layer mixing layer. The  $J(O^1D)$  increases from  $8.9 \times 10^{-3} \text{ s}^{-1}$  to  $14.3 \times 10^{-3} \text{ s}^{-1}$  and  $J(NO_2)$  increases from  $3.0 \times 10^{-5} \text{ s}^{-1}$  to  $6.2 \times 10^{-5} \text{ s}^{-1}$  in the boundary layer mixing layer. The corresponding [OH] increased from  $6.2 \times 10^6 \text{ cm}^{-3}$  to  $11.9 \times 10^6 \text{ cm}^{-3}$  based equation 4. Thus, the [OH] at the top of the boundary layer mixing layer is two times of that on the ground surface due to the variation in photolysis rate. Our estimated [OH] at the surface is consistent with the previously estimated relationships between the [OH] and  $J(O^1D)$  (Rohrer and Berresheim, 2006).

Overall, the aerosol profiles tend to be uniformly distributed within the boundary layer mixing layer due to the strong turbulence in the afternoon. The corresponding estimated  $J(O^1D)$ , and  $J(NO_2)$  values increase with altitude, which leads to higher [OH] at the top of the boundary layer mixing layer than that at the ground. Therefore, the  $[H_2SO_4]$  should increase with altitude based on equation 42. There should be more nucleation processing at the top of the boundary layer mixing layer than that at the ground, which is consistent with our field measurement. ~~The schematic graph of the influence of aerosol-radiation interaction on NPF is shown in Fig. 6.~~

### 3.4 Impact of ~~Boundary layer~~Mixing layer development on the photolysis rates

For a better understanding of the aerosol-radiation interaction on NPF, we estimated the photolysis rates under different aerosol vertical profiles. Based on the work of Liu et al. (2009), two typical types of aerosol profiles exist under different ~~boundary layer~~mixing layer as shown in Fig. S4. For the first type of ~~boundary layer~~mixing layer, aerosols were not well mixed within the ~~boundary layer~~mixing layer and the aerosol number concentrations decrease with altitude exponentially (type A). Another type of ~~boundary layer~~mixing layer has aerosol number concentration constant in the ~~boundary layer~~mixing layer and then decreasing with altitude above the boundary (type B). For type B, we estimated the corresponding photolysis rate for different ~~boundary layer~~mixing layer heights between 500 m and 1000 m, which covers the mean ~~boundary layer~~mixing layer altitude in the North China Plain (Zhu et al., 2018). The different aerosol optical depth (AOD), which ranges between 0.3 and 2, are used for different pollution conditions.

Four different aerosol profiles are used in this study. Details of the four different aerosol profiles are summarized in Table 2. The first one corresponds to the aerosol ~~boundary layer~~mixing layer type A, with a exact boundary altitude of 1000 m and AOD of 0.3 (B1). The second aerosol profile has the same boundary altitude of 1000m and AOD of 0.3, but the ~~boundary layer~~mixing layer type is changed into B (B2). The third aerosol profile also corresponds to ~~boundary layer~~mixing layer type B, and a ~~boundary layer~~mixing layer altitude of 1000m, but the AOD is 0.8 (B3). The last one has a ~~boundary layer~~mixing layer altitude of 500m, with an AOD of 0.8 and a ~~boundary layer~~mixing layer type of B (B4).

The  $J(O^1D)$ , and  $J(NO_2)$  profiles under the above-mentioned aerosol profiles are estimated and shown in Fig. 5 (a) and (b). For each type, both the  $J(O^1D)$ , and  $J(NO_2)$  increase with altitude. The increased ratio of the  $J(O^1D)$  with altitude ( $k_{O^1D}$ ) are  $1.7 \times 10^{-5}$ ,  $2.0 \times 10^{-5}$ ,  $3.0 \times 10^{-5}$ , and  $5.4 \times 10^{-5}$  s<sup>-1</sup>km<sup>-1</sup>, for the aerosol profile of B1, B2, B3, and B4 respectively. The corresponding increase ratio of the  $J(NO_2)$  with altitude ( $k_{NO_2}$ ) are  $2.6 \times 10^{-3}$ ,  $3.3 \times 10^{-3}$ ,  $5.3 \times 10^{-3}$ , and  $9.0 \times 10^{-3}$  s<sup>-1</sup>km<sup>-1</sup>, for B1, B2, B3, and B4, respectively. The increase ratio of [OH] were estimated to be  $3.4 \times 10^6$ ,  $4.1 \times 10^6$ ,  $5.5 \times 10^6$ , and  $7.4 \times 10^6$  cm<sup>-3</sup>km<sup>-1</sup> for B1, B2, B3 and B4, respectively (Table 2).

These four profiles represent the typical ambient aerosol profiles in the early morning, late morning, early afternoon, and late afternoon, respectively. In the early morning, the turbulence in the boundary layer mixing layer is weak and the aerosol within the boundary layer mixing layer is not well mixed (B1). In the late morning, the aerosol in the boundary is well mixed and uniformly distributed due to the increasing turbulence (B2). The early afternoon (B3) should have higher AOD when compared with that in the late morning due to the formation of the secondary aerosol. However, the boundary layer mixing layer altitude decreased in the late afternoon (B4) because the turbulence within the boundary layer mixing layer weakened compared with B3. The ambient aerosol profiles tend to change from B1 to B4 from early morning to late afternoon. The corresponding  $k_{O^1D}$  and  $k_{NO_2}$  increased with the development of the boundary layer mixing layer. In the late afternoon, the difference of photolysis rate at the top of the boundary layer mixing layer and ground are largest. Furthermore, the turbulence in the mixing layer is weakened and the nucleation formed particles cannot be mixed down to the ground. Therefore, it is more likely to observe more nucleation mode



particles at the top of the ~~boundary layer~~mixing layer than at the ground in the late afternoon, which is consistent with our measurement.

#### 4. Conclusion

330 In this study, we characterized the aerosol PNSD at different times and different altitudes based on field measurements at an urban site, in Beijing, China. Our measurements show that the aerosol size distribution profiles varied significantly with the development of the ~~boundary layer~~mixing layer.

In the morning, the turbulence in the boundary was weak and the initial emitted particles cannot  
335 be mixed to a higher layer. The corresponding aerosol PNSD at the surface was larger than that at higher locations. At noon, the particles within the boundary were well mixed and tend to be uniformly distributed at different altitudes. In the late afternoon, we found more nucleation mode particles at a higher altitude than that at the ground. The larger partitions of nucleation mode particles do not result from transformation. We concluded that the nucleation processing in the upper  
340 ~~boundary layer~~mixing layer ~~were~~was more likely to happen than that at the ground.

The TUV model was employed to estimate the profile of photolysis rate for different aerosol profiles. Results showed that both the  $J(O^1D)$ , and  $J(NO_2)$  values increased with altitude, which led to higher [OH] at the top of the ~~boundary layer~~mixing layer than that at the ground. The corresponding [H<sub>2</sub>SO<sub>4</sub>] should increase with altitude based on equation ~~4~~2, when the aerosol was  
345 well mixed and uniformed in the ~~mixed layer~~mixing layer. Therefore, more nucleation processing at

the top of the boundary layer mixing layer may happen than that at the ground, which is consistent with our field measurement.

We also estimate the corresponding photolysis rate profile under different boundary structures.

The increasing ratio of the photolysis rate with altitude increase with the development of the boundary layer mixing layer from early morning to late afternoon. In the late afternoon, the difference of the photolysis rate at the upper boundary layer mixing layer and that at the ground are the largest.

At the same time, the turbulence is not so strong that the nucleation mode particles formed in the upper boundary layer mixing layer are not able to mix down to the ground. Therefore, it is a favor to observe higher nucleation mode particles concentration at the upper boundary layer mixing layer than

that at the ground in the afternoon. Our study reveals that the vertical distribution of ambient aerosols would first influence the vertical profile of the photolysis rate. Then the NPF for different altitudes is tuned due to the different photolysis rates.

**Data availability.** The data is available upon request to the corresponding author.

**Author contributions.** Gang Zhao and Yishu Zhu did the analysis and wrote the manuscript. Min Hu, Chunsheng Zhao, Zhijun Wu, Xin Fang, and Gang Zhao discussed the results. Yishu Zhu, Jingchuan Chen, Taomou Zong, Tianyi Tan, Keding Lu, and Haichao Wang conducted the measurements.

**Competing interests.** The authors declare that they have no conflict of interest.

**Acknowledgments.** This work is supported by the National Natural Science Foundation of China (91844301) and the National Key Research and Development Program of China (2016YFC0202000 Task 3, 5).



## References

- 370 Bohren, C. F., and Huffman, D. R.: Absorption and Scattering by a Sphere, in: Absorption and Scattering of Light by Small Particles, Wiley-VCH Verlag GmbH, 82-129, 2007.
- Bullard, R. L., Singh, A., Anderson, S. M., Lehmann, C. M. B., and Stanier, C. O.: 10-Month characterization of the aerosol number size distribution and related air quality and meteorology at the Bondville, IL Midwestern background site, Atmospheric Environment,
- 375 <http://dx.doi.org/10.1016/j.atmosenv.2016.12.055>.
- Chen, C., Sun, Y. L., Xu, W. Q., Du, W., Zhou, L. B., Han, T. T., Wang, Q. Q., Fu, P. Q., Wang, Z. F., Gao, Z. Q., Zhang, Q., and Worsnop, D. R.: Characteristics and sources of submicron aerosols above the urban canopy (260 m) in Beijing, China, during the 2014 APEC summit, Atmospheric Chemistry and Physics, 15, 12879-12895, 10.5194/acp-15-12879-2015, 2015.
- 380 Chen, H., Hodshire, A. L., Ortega, J., Greenberg, J., McMurry, P. H., Carlton, A. G., Pierce, J. R., Hanson, D. R., and Smith, J. N.: Vertically resolved concentration and liquid water content of atmospheric nanoparticles at the US DOE Southern Great Plains site, Atmospheric Chemistry and Physics, 18, 311-326, 10.5194/acp-18-311-2018, 2018.
- Du, P., Gui, H., Zhang, J., Liu, J., Yu, T., Wang, J., Cheng, Y., and Shi, Z.: Number size distribution
- 385 of atmospheric particles in a suburban Beijing in the summer and winter of 2015, Atmospheric Environment, 186, 32-44, 10.1016/j.atmosenv.2018.05.023, 2018.
- Du, W., Zhao, J., Wang, Y., Zhang, Y., Wang, Q., Xu, W., Chen, C., Han, T., Zhang, F., Li, Z., Fu, P., Li, J., Wang, Z., and Sun, Y.: Simultaneous measurements of particle number size distributions at ground level and 260 m on a meteorological tower in urban Beijing, China, Atmos. Chem. Phys., 17,
- 390 6797-6811, 10.5194/acp-17-6797-2017, 2017.
- Ehhalt, D. H., and Rohrer, F.: Dependence of the OH concentration on solar UV, Journal of Geophysical Research: Atmospheres, 105, 3565-3571, <https://doi.org/10.1029/1999JD901070>, 2000.
- Elterman, L., Wexler, R., and Chang, D.: COMPARISON OF AEROSOL MEASUREMENTS OVER NEW MEXICO WITH ATMOSPHERIC FEATURES, Journal of the Optical Society of
- 395 America, 58, 741-&, 1968.

- Ferrero, L., Mocnik, G., Ferrini, B. S., Perrone, M. G., Sangiorgi, G., and Bolzacchini, E.: Vertical profiles of aerosol absorption coefficient from micro-Aethalometer data and Mie calculation over Milan, *Science of the Total Environment*, 409, 2824-2837, 2011.
- Ghan, S. J., and Schwartz, S. E.: Aerosol Properties and Processes: A Path from Field and Laboratory Measurements to Global Climate Models, *Bulletin of the American Meteorological Society*, 88, 1059-1084, 10.1175/bams-88-7-1059, 2007.
- Kulmala, and Markku: Direct Observations of Atmospheric Aerosol Nucleation, *Science*, 2013.
- Kulmala, M., Maso, M. D., Mäkelä, J. M., Pirjola, L., Väkevä, M., Aalto, P., Mäkeläinen, P., Hämeri, K., and O’dwod, C. D.: On the formation, growth and composition of nucleation mode particles, *Tellus B: Chemical and Physical Meteorology*, 53, 479-490, 10.3402/tellusb.v53i4.16622, 2001.
- Kulmala, M., Vehkamäki, H., Petaja, T., Dal Maso, M., Lauri, A., Kerminen, V. M., Birmili, W., and McMurry, P. H.: Formation and growth rates of ultrafine atmospheric particles: a review of observations, *Journal of Aerosol Science*, 35, 143-176, 10.1016/j.jaerosci.2003.10.003, 2004.
- Kulmala, M., Petäjä, T., Ehn, M., Thornton, J., Sipilä, M., Worsnop, D. R., and Kerminen, V. M.: Chemistry of Atmospheric Nucleation: On the Recent Advances on Precursor Characterization and Atmospheric Cluster Composition in Connection with Atmospheric New Particle Formation, *Annual Review of Physical Chemistry*, 65, 21-37, 10.1146/annurev-physchem-040412-110014, 2014.
- Liu, P., Zhao, C., Zhang, Q., Deng, Z., Huang, M., Xincheng, M. A., and Tie, X.: Aircraft study of aerosol vertical distributions over Beijing and their optical properties, *Tellus Series B-Chemical & Physical Meteorology*, 61, 756–767, 2009.
- Madronich, S., and Flocke, S.: Theoretical Estimation of Biologically Effective UV Radiation at the Earth’s Surface, in: *Solar Ultraviolet Radiation*, Berlin, Heidelberg, 1997, 23-48.
- Malinina, E., Rozanov, A., Rozanov, V., Liebing, P., Bovensmann, H., and Burrows, J. P.: Aerosol particle size distribution in the stratosphere retrieved from SCIAMACHY limb measurements, *Atmospheric Measurement Techniques Discussions*, 1-29, 10.5194/amt-2017-388, 2017.

- Maso, M. D., Kulmala, M., Riipinen, I., Wagner, R., Hussein, T., Aalto, P. P., and Lehtinen, K. E. J.: Formation and growth of fresh atmospheric aerosols: eight years of aerosol size distribution data from SMEAR II, Hyytiälä, Finland, *Boreal Environment Research*, 10, 323-336, 2005.
- 425 Merikanto, J., Spracklen, D. V., Mann, G. W., Pickering, S. J., and Carslaw, K. S.: Impact of nucleation on global CCN, *Atmospheric Chemistry and Physics*, 9, 8601-8616, 10.5194/acp-9-8601-2009, 2009.
- Müller, T., Laborde, M., Kassell, G., and Wiedensohler, A.: Design and performance of a three-wavelength LED-based total scatter and backscatter integrating nephelometer, *Atmos. Meas.*  
 430 *Tech.*, 4, 1291-1303, 10.5194/amt-4-1291-2011, 2011.
- Peng, Y., Liu, X., Dai, J., Wang, Z., Dong, Z., Dong, Y., Chen, C., Li, X., Zhao, N., and Fan, C.: Aerosol size distribution and new particle formation events in the suburb of Xi'an, northwest China, *Atmospheric Environment*, 153, 194-205, 10.1016/j.atmosenv.2017.01.022, 2017.
- Platis, A., Altstädter, B., Wehner, B., Wildmann, N., Lampert, A., Hermann, M., Birmili, W., and  
 435 Bange, J.: An Observational Case Study on the Influence of Atmospheric Boundary-Layer Dynamics on New Particle Formation, *Boundary-Layer Meteorology*, 158, 67-92, 10.1007/s10546-015-0084-y, 2016.
- Qi, X., Ding, A., Nie, W., Chi, X., Huang, X., Xu, Z., Wang, T., Wang, Z., Wang, J., Sun, P., Zhang, Q., Huo, J., Wang, D., Bian, Q., Zhou, L., Zhang, Q., Ning, Z., Fei, D., Xiu, G., and Fu, Q.: Direct  
 440 measurement of new particle formation based on tethered airship around the top of the planetary boundary layer in eastern China, *Atmospheric Environment*, 209, 92-101, 10.1016/j.atmosenv.2019.04.024, 2019.
- Rohrer, F., and Berresheim, H.: Strong correlation between levels of tropospheric hydroxyl radicals and solar ultraviolet radiation, *Nature*, 442, 184-187, 10.1038/nature04924, 2006.
- 445 Schobesberger, S., Vaananen, R., and Leino, K.: Airborne measurements over the boreal forest of southern Finland during new particle formation events in 2009 and 2010, *Boreal Environment Research*, 2013.

- Shang, D., Hu, M., Zheng, J., Qin, Y., Du, Z., Li, M., Fang, J., Peng, J., Wu, Y., Lu, S., and Guo, S.: Particle number size distribution and new particle formation under the influence of biomass burning at a high altitude background site at Mt. Yulong (3410 m), China, *Atmospheric Chemistry and Physics*, 18, 15687-15703, 10.5194/acp-18-15687-2018, 2018.
- Shang, D., Peng, J., Guo, S., Wu, Z., and Hu, M.: Secondary aerosol formation in winter haze over the Beijing-Tianjin-Hebei Region, China, *Frontiers of Environmental Science & Engineering*, 15, 10.1007/s11783-020-1326-x, 2020.
- Steinfeld, J. I.: *Atmospheric Chemistry and Physics: From Air Pollution to Climate Change, Environment: Science and Policy for Sustainable Development*, 40, 26-26, 10.1080/00139157.1999.10544295, 1998.
- Stolzenburg, M. R., McMurry, P. H., Sakurai, H., Smith, J. N., Mauldin III, R. L., Eisele, F. L., and Clement, C. F.: Growth rates of freshly nucleated atmospheric particles in Atlanta, *Journal of Geophysical Research: Atmospheres*, 110, <https://doi.org/10.1029/2005JD005935>, 2005.
- Tao, J. C., Zhao, C. S., Ma, N., and Liu, P. F.: The impact of aerosol hygroscopic growth on the single-scattering albedo and its application on the NO<sub>2</sub> photolysis rate coefficient, *Atmos. Chem. Phys.*, 14, 12055-12067, 10.5194/acp-14-12055-2014, 2014.
- Wang, H., Lu, K., Chen, X., Zhu, Q., Wu, Z., Wu, Y., and Sun, K.: Fast particulate nitrate formation via  $\text{N}_2\text{O}_5$  uptake aloft in winter in Beijing, *Atmospheric Chemistry and Physics*, 18, 10483-10495, 10.5194/acp-18-10483-2018, 2018a.
- Wang, J., Krejci, R., Giangrande, S., Kuang, C., Barbosa, H. M., Brito, J., Carbone, S., Chi, X., Comstock, J., Ditas, F., Lavric, J., Manninen, H. E., Mei, F., Moran-Zuloaga, D., Pohlker, C., Pohlker, M. L., Saturno, J., Schmid, B., Souza, R. A., Springston, S. R., Tomlinson, J. M., Toto, T., Walter, D., Wimmer, D., Smith, J. N., Kulmala, M., Machado, L. A., Artaxo, P., Andreae, M. O., Petaja, T., and Martin, S. T.: Amazon boundary layer aerosol concentration sustained by vertical transport during rainfall, *Nature*, 539, 416-419, 10.1038/nature19819, 2016.
- Wang, Q., Sun, Y., Xu, W., Du, W., Zhou, L., Tang, G., Chen, C., Cheng, X., Zhao, X., Ji, D., Han, T., Wang, Z., Li, J., and Wang, Z.: Vertically resolved characteristics of air pollution during two

475 severe winter haze episodes in urban Beijing, China, *Atmospheric Chemistry and Physics*, 18, 2495-2509, 10.5194/acp-18-2495-2018, 2018b.

Weber, R. J., Marti, J. J., McMurry, P. H., Eisele, F. L., Tanner, D. J., and Jefferson, A.: MEASURED ATMOSPHERIC NEW PARTICLE FORMATION RATES: IMPLICATIONS FOR NUCLEATION MECHANISMS, *Chemical Engineering Communications*, 151, 53-64, 480 10.1080/00986449608936541, 1996.

Weber, R. J., Marti, J. J., McMurry, P. H., Eisele, F. L., Tanner, D. J., and Jefferson, A.: Measurements of new particle formation and ultrafine particle growth rates at a clean continental site, *Journal of Geophysical Research: Atmospheres*, 102, 4375-4385, <https://doi.org/10.1029/96JD03656>, 1997.

485 Weber, R. J., Chen, G., Davis, D. D., Mauldin, R. L., Tanner, D. J., Eisele, F. L., Clarke, A. D., Thornton, D. C., and Bandy, A. R.: Measurements of enhanced H<sub>2</sub>SO<sub>4</sub> and 3-4 nm particles near a frontal cloud during the First Aerosol Characterization Experiment (ACE 1), *J Geophys Res-Atmos*, 106, 24107-24117, 10.1029/2000jd000109, 2001.

Williamson, C. J., Kupc, A., Axisa, D., Bilsback, K. R., Bui, T., Campuzano-Jost, P., Dollner, M., 490 Froyd, K. D., Hodshire, A. L., Jimenez, J. L., Kodros, J. K., Luo, G., Murphy, D. M., Nault, B. A., Ray, E. A., Weinzierl, B., Wilson, J. C., Yu, F., Yu, P., Pierce, J. R., and Brock, C. A.: A large source of cloud condensation nuclei from new particle formation in the tropics, *Nature*, 574, 399-403, 10.1038/s41586-019-1638-9, 2019.

Wu, Z., Hu, M., Lin, P., Liu, S., Wehner, B., and Wiedensohler, A.: Particle number size distribution 495 in the urban atmosphere of Beijing, China, *Atmospheric Environment*, 42, 7967-7980, <https://doi.org/10.1016/j.atmosenv.2008.06.022>, 2008.

Zhang, R. Y., Khalizov, A., Wang, L., Hu, M., and Xu, W.: Nucleation and Growth of Nanoparticles in the Atmosphere, *Chemical Reviews*, 112, 1957-2011, 10.1021/cr2001756, 2012.

Zhao, B., Shrivastava, M., Donahue, N. M., Gordon, H., Schervish, M., Shilling, J. E., Zaveri, R. A., 500 Wang, J., Andreae, M. O., Zhao, C., Gaudet, B., Liu, Y., Fan, J., and Fast, J. D.: High concentration



of ultrafine particles in the Amazon free troposphere produced by organic new particle formation, *Proceedings of the National Academy of Sciences*, 117, 25344, 10.1073/pnas.2006716117, 2020.

Zhao, G., Zhao, C., Kuang, Y., Tao, J., Tan, W., Bian, Y., Li, J., and Li, C.: Impact of aerosol hygroscopic growth on retrieving aerosol extinction coefficient profiles from elastic-backscatter lidar signals, *Atmospheric Chemistry and Physics*, 17, 12133-12143, 10.5194/acp-17-12133-2017, 2017.

Zhao, G., Zhao, C., Kuang, Y., Bian, Y., Tao, J., Shen, C., and Yu, Y.: Calculating the aerosol asymmetry factor based on measurements from the humidified nephelometer system, *Atmospheric Chemistry and Physics*, 18, 9049-9060, 10.5194/acp-18-9049-2018, 2018.

Zhao, G., Tao, J., Kuang, Y., Shen, C., Yu, Y., and Zhao, C.: Role of black carbon mass size distribution in the direct aerosol radiative forcing, *Atmos. Chem. Phys.*, 19, 13175-13188, 10.5194/acp-19-13175-2019, 2019.

Zhu, X., Tang, G., Guo, J., Hu, B., Song, T., Wang, L., Xin, J., Gao, W., Munkel, C., Schäfer, K., Li, X., and Wang, Y.: Mixing layer height on the North China Plain and meteorological evidence of serious air pollution in southern Hebei, *Atmospheric Chemistry and Physics*, 18, 4897-4910, 10.5194/acp-18-4897-2018, 2018.

Zhu, Y., Wu, Z., Park, Y., Fan, X., Bai, D., Zong, P., Qin, B., Cai, X., and Ahn, K. H.: Measurements of atmospheric aerosol vertical distribution above North China Plain using hexacopter, *Sci Total Environ*, 665, 1095-1102, 10.1016/j.scitotenv.2019.02.100, 2019.

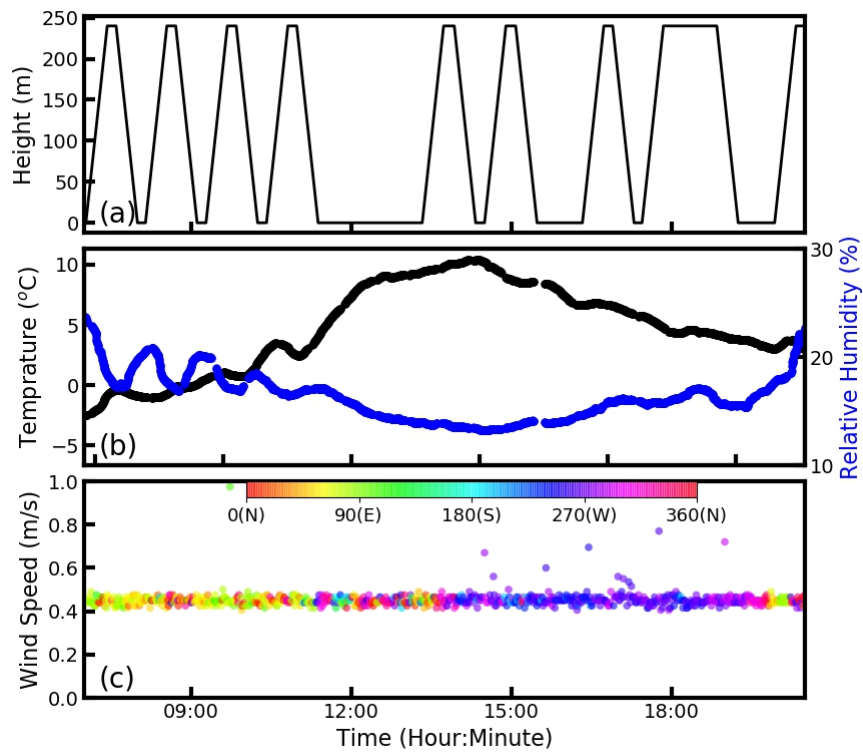


**Figure 1.** Time series of (a) the measurement altitude, (b) temperature (black line) and relative humidity (blue line), and (c) the wind speed and wind direction.

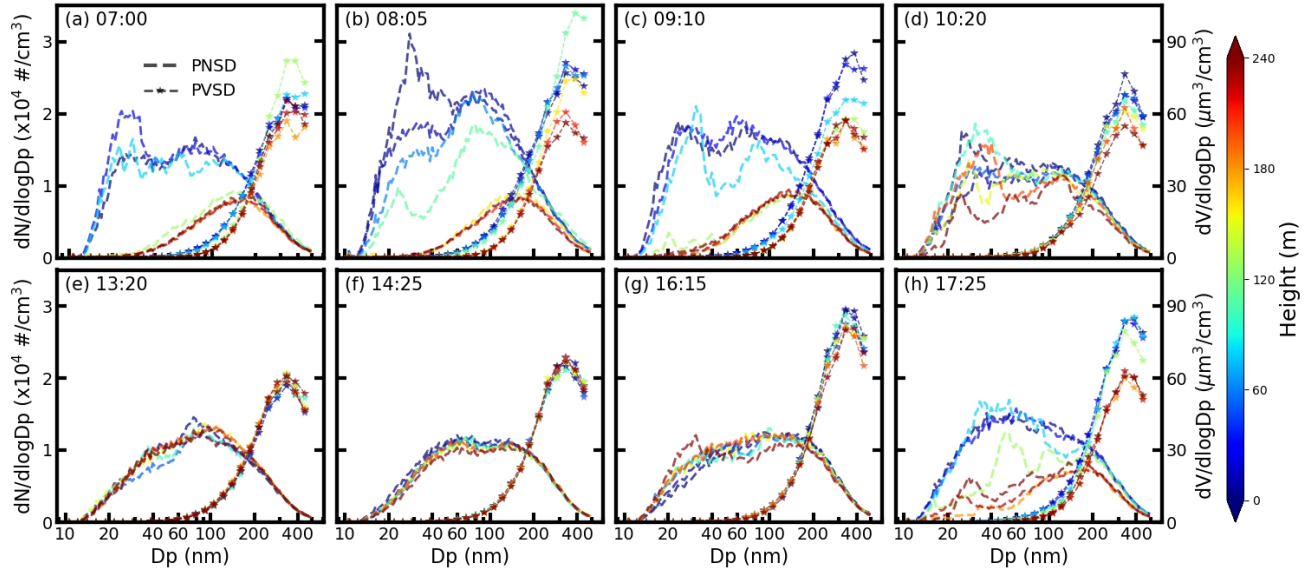


**Figure. 2.** The measured aerosol PSND (dashed line) and the PVSD (dashed line with star) at (a) 7:00, (b) 8:05, (c) 9:50, (d) 10:20, (e) 13:20, (f) 14:25, (g) 16:15, and (h) 17:25. The filled colors represent the corresponding measurement altitude above the ground.

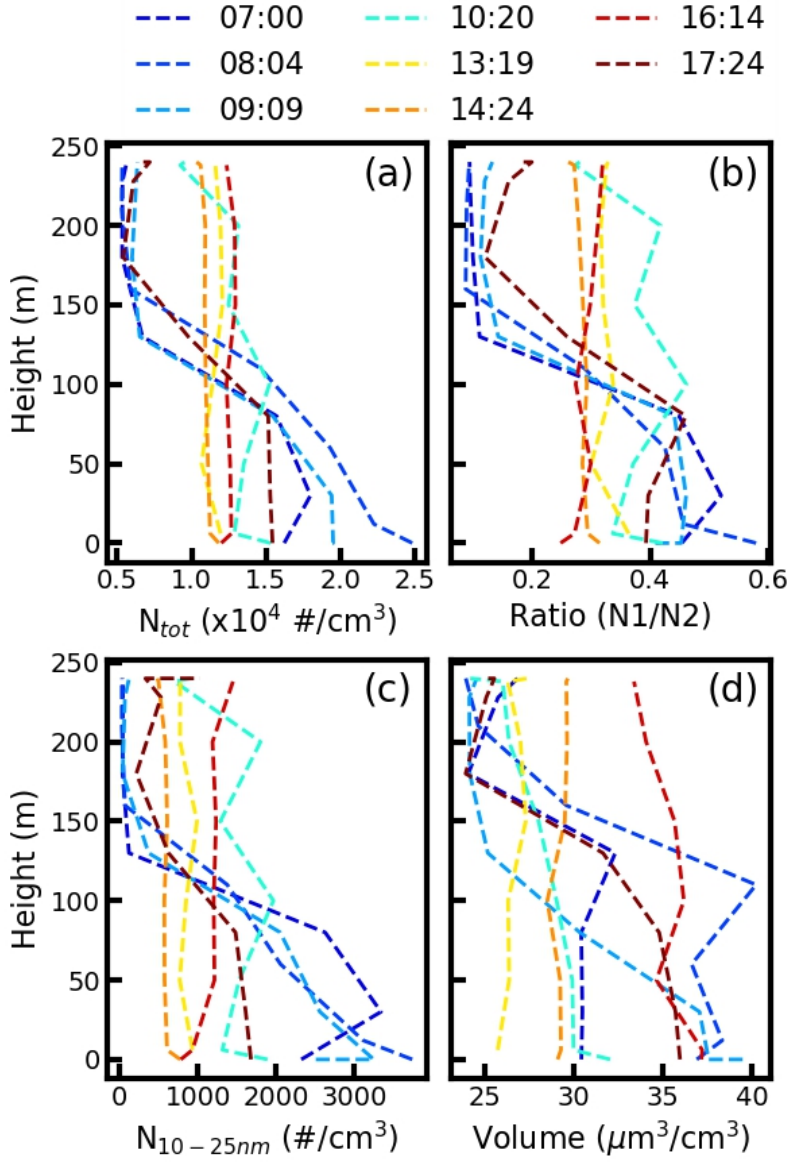


**Figure 3.** The measured (a) aerosol number concentrations, (b) number ratio of the nucleation mode aerosol number concentrations to Aitken mode aerosol number concentrations, (c) aerosol number concentrations for 10-25 nm, and (d) measured aerosol volume concentrations at different altitudes.

The filled colors of different lines denote the different measurement times.

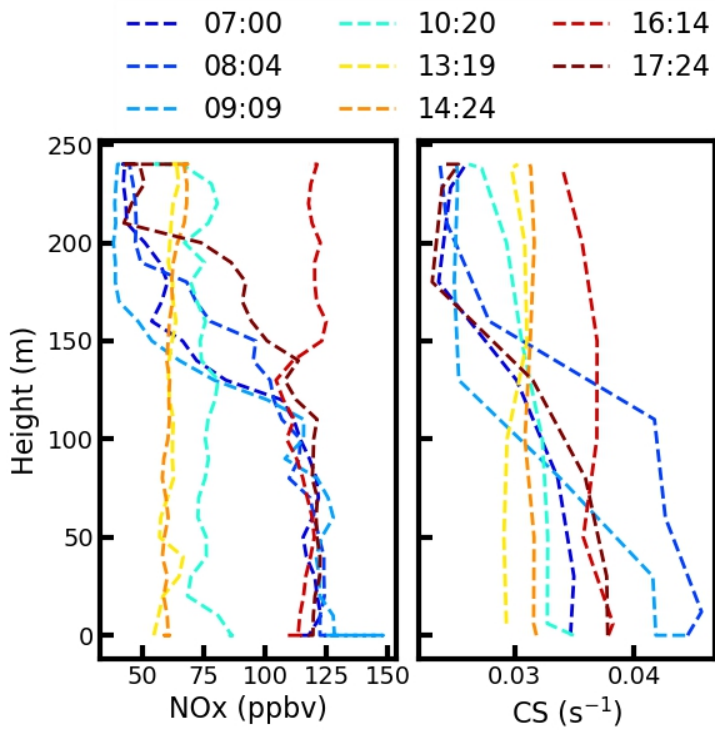
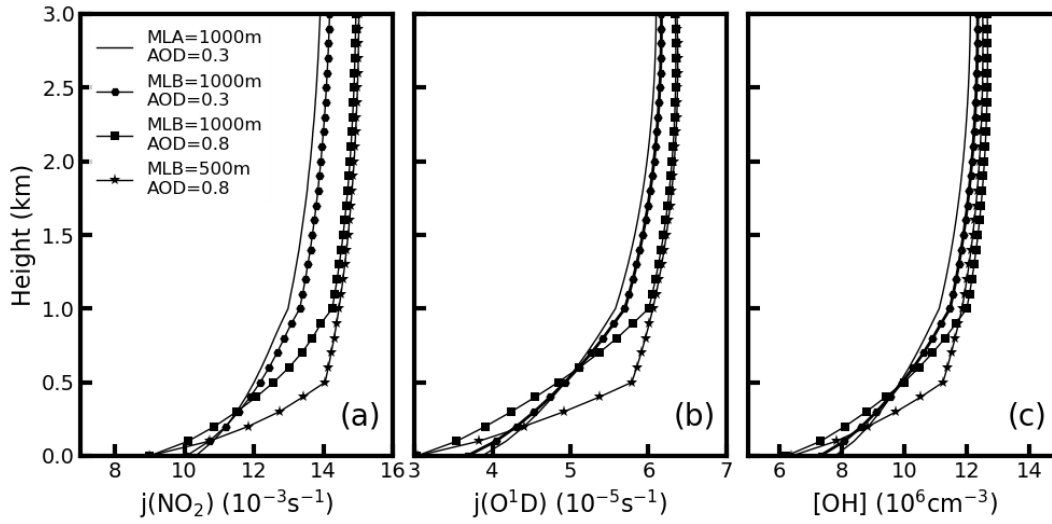


**Figure. 4.** The measured (a) NO<sub>x</sub> and (b) CS at different altitudes. The filled colors of different lines denote the different measurement times.



540 **Figure. 5.** The estimated (a)  $j(\text{NO}_2)$ , (b)  $j(\text{O}^1\text{D})$ , and (c) OH concentration for different aerosol  
 profiles. The (1) solid line, (2) solid line marked with hexagon, (3) solid line marked with squares,  
 and (4) solid line marked with stars represent the aerosol distribution of B1, B2, B3, and B4,  
 respectively.

545

**Table 1.**

The  
number  
ratio of  
nucleati  
on mode  
to Aiken  
mode.

<b>Time</b> <b>Altitude</b>	<b>7:00</b>	<b>8:05</b>	<b>9:10</b>	<b>10:20</b>	<b>13:20</b>	<b>14:25</b>	<b>16:15</b>	<b>17:25</b>
<b>0</b>	<b>0.56</b>	<b>0.52</b>	<b>0.43</b>	<b>0.36</b>	<b>0.21</b>	<b>0.20</b>	<b>0.21</b>	<b>0.32</b>
<b>30</b>	<b>0.63</b>	<b>0.44</b>	<b>0.42</b>	<b>0.35</b>	<b>0.21</b>	<b>0.19</b>	<b>0.23</b>	<b>0.30</b>
<b>60</b>	<b>0.61</b>	<b>0.34</b>	<b>0.40</b>	<b>0.40</b>	<b>0.22</b>	<b>0.19</b>	<b>0.27</b>	<b>0.28</b>
<b>110</b>	<b>0.05</b>	<b>0.26</b>	<b>0.25</b>	<b>0.46</b>	<b>0.27</b>	<b>0.19</b>	<b>0.28</b>	<b>0.14</b>
<b>160</b>	<b>0.04</b>	<b>0.03</b>	<b>0.07</b>	<b>0.39</b>	<b>0.20</b>	<b>0.17</b>	<b>0.27</b>	<b>0.17</b>
<b>210</b>	<b>0.03</b>	<b>0.03</b>	<b>0.08</b>	<b>0.51</b>	<b>0.20</b>	<b>0.17</b>	<b>0.30</b>	<b>0.31</b>
<b>240</b>	<b>0.04</b>	<b>0.03</b>	<b>0.09</b>	<b>0.26</b>	<b>0.21</b>	<b>0.16</b>	<b>0.34</b>	<b>0.37</b>

**Table 2.** Details of the aerosol optical profiles and estimated photolysis values.

Profile	Type <sup>*1</sup>	Altitude <sup>*2</sup>	AOD	k [J(NO <sub>2</sub> )] (10 <sup>-3</sup> s <sup>-1</sup> km <sup>-1</sup> )	k [J(O <sup>1</sup> D)] (10 <sup>-5</sup> s <sup>-1</sup> km <sup>-1</sup> )	k [OH] (10 <sup>6</sup> cm <sup>-3</sup> km <sup>-1</sup> )
B1	A	1000	0.3	2.6	1.7	3.4
B2	B	1000	0.3	3.3	2.0	4.1
B3	B	1000	0.8	5.3	3.0	5.5
B4	B	500	0.8	9.0	5.4	7.4

<sup>\*1</sup>Boundary layer Type.

<sup>\*2</sup>Boundary layer altitude.



Supplement for

## **Impact of aerosol-radiation interaction on the new particle formation**

Gang Zhao<sup>1</sup>, Yishu Zhu<sup>1</sup>, Zhiju Wu<sup>1</sup>, Taomou Zong<sup>1</sup>, Jingchuan Chen<sup>1</sup>, Tianyi Tian<sup>1</sup>, Haichao Wang<sup>1</sup>, Xin Fang<sup>1</sup>, Keding Lu<sup>1</sup>, Chunsheng Zhao<sup>2</sup>, Min Hu<sup>1\*</sup>

1 State Key Joint Laboratory of Environmental Simulation and Pollution Control, International Joint Laboratory for Regional Pollution Control, Ministry of Education, College of Environmental Sciences and Engineering, Peking University, Beijing, 100871, China

2 Department of Atmospheric and Oceanic Sciences, School of Physics, Peking University, Beijing, 100871, China

### **1. Lognormal fit of the measured PNSD.**

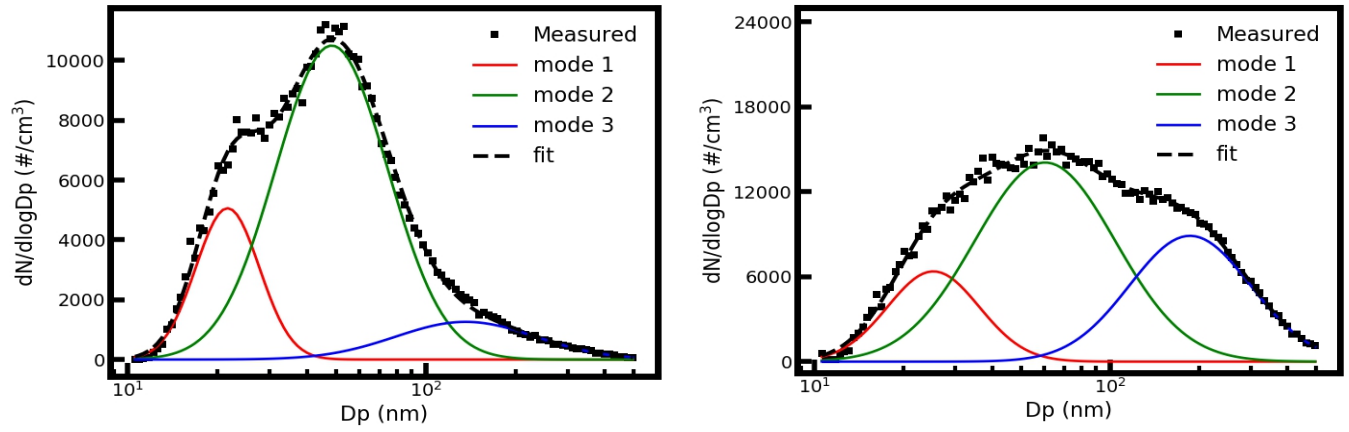


**Figure. S1.** Lognormal fit (three modes) examples of the PNSD during the campaign. Black squares mark the measured PNSD, dashed lines represent the PNSD of fitting modes, and the black dashed line marks the sum of the PNSD of all fitting three modes. Mode 1 (red), 2 (green), and 3 (blue) are nucleation mode, Aitken mode, and accumulation mode, respectively.

## 2 Comparison between the measured and calculated scattering coefficients

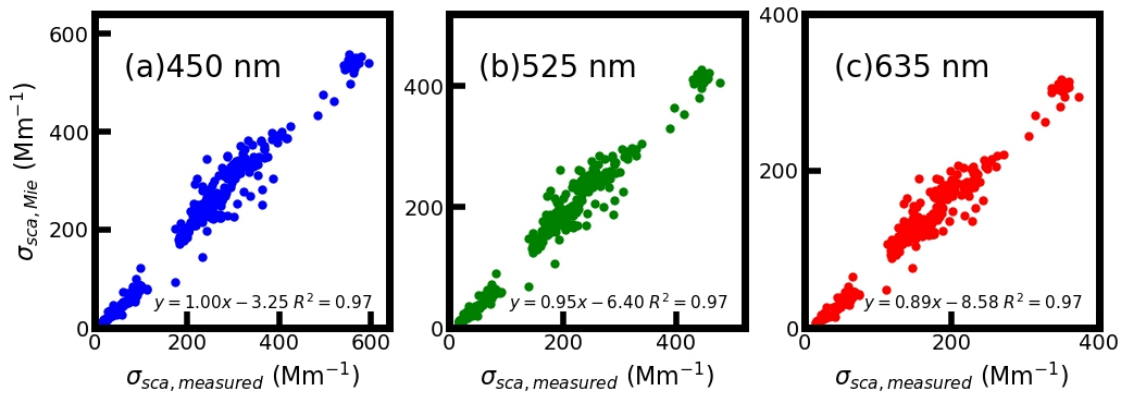


**Fig. S2.** Comparison between the measured scattering coefficients and calculated scattering coefficients at the wavelength of (a) 450 nm, (b) 525 nm, and (c) 635 nm.

### 3 Measured PNSD profile when the cabin is moving downward.

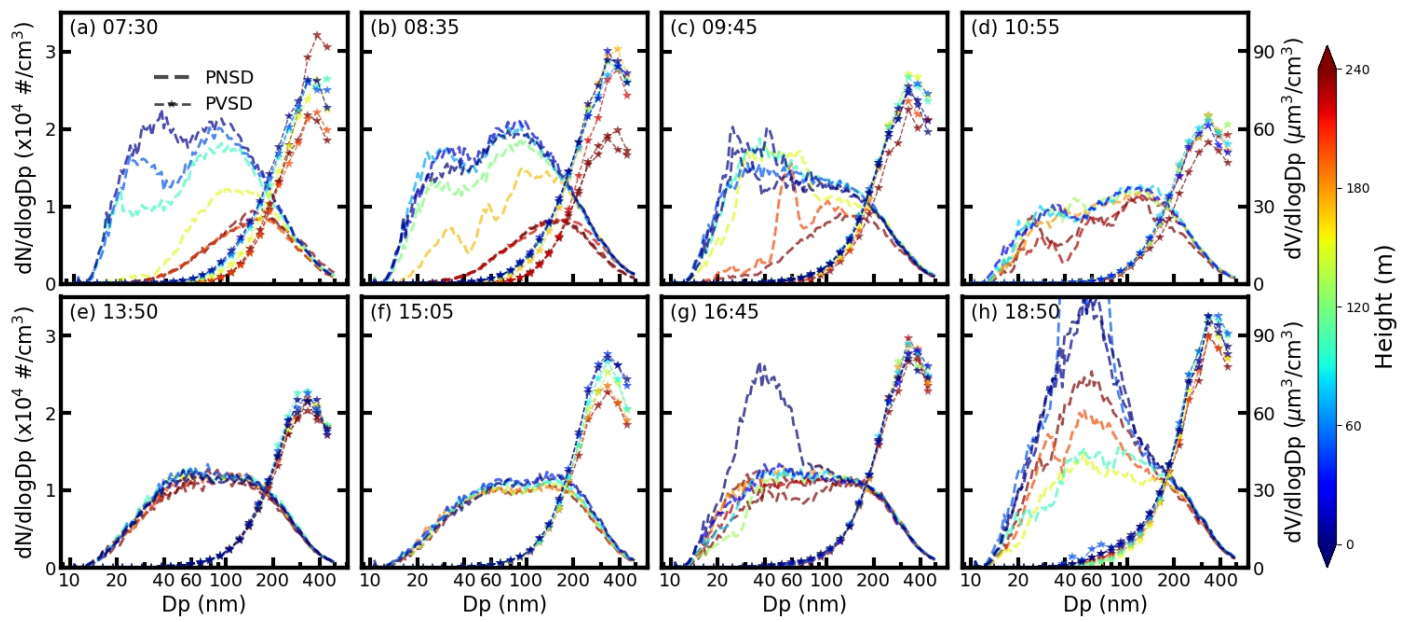


**Figure. S3.** The measured aerosol PNSD (dashed line) and the PVSD (dashed line with star) at (a) 7:00, (b) 8:05, (c) 9:50, (d) 10:20, (e) 13:20, (f) 14:25, (g) 16:15, and (h) 17:25. The filled colors represent the corresponding measurement height above the ground.

#### 4 Different aerosol number concentration distribution types.

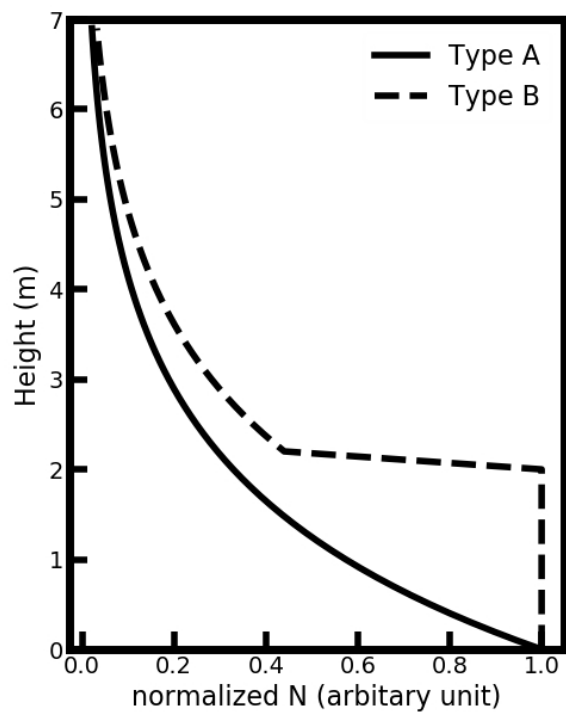


**Figure S4.** The typical aerosol number concentration (N) at different heights for types A and B.